SUPPORTING INFORMATION

Guest Migration Revealed in CO_2 Clathrate Hydrates

A.N. Salamatin[1], A. Falenty[2], T.C. Hansen[3] and W.F. Kuhs[2]*

[1] Dept. of Applied Mathematics, Kazan (Volga Region) Federal University, Kazan 420008, Russia

[2] GZG, Abt. Kristallographie, Universität Göttingen, Goldschmidtstrasse 1, 37077 Göttingen, Germany

[3] Institut Laue-Langevin (ILL), 71 avenue des Martyrs, 38000 Grenoble, France

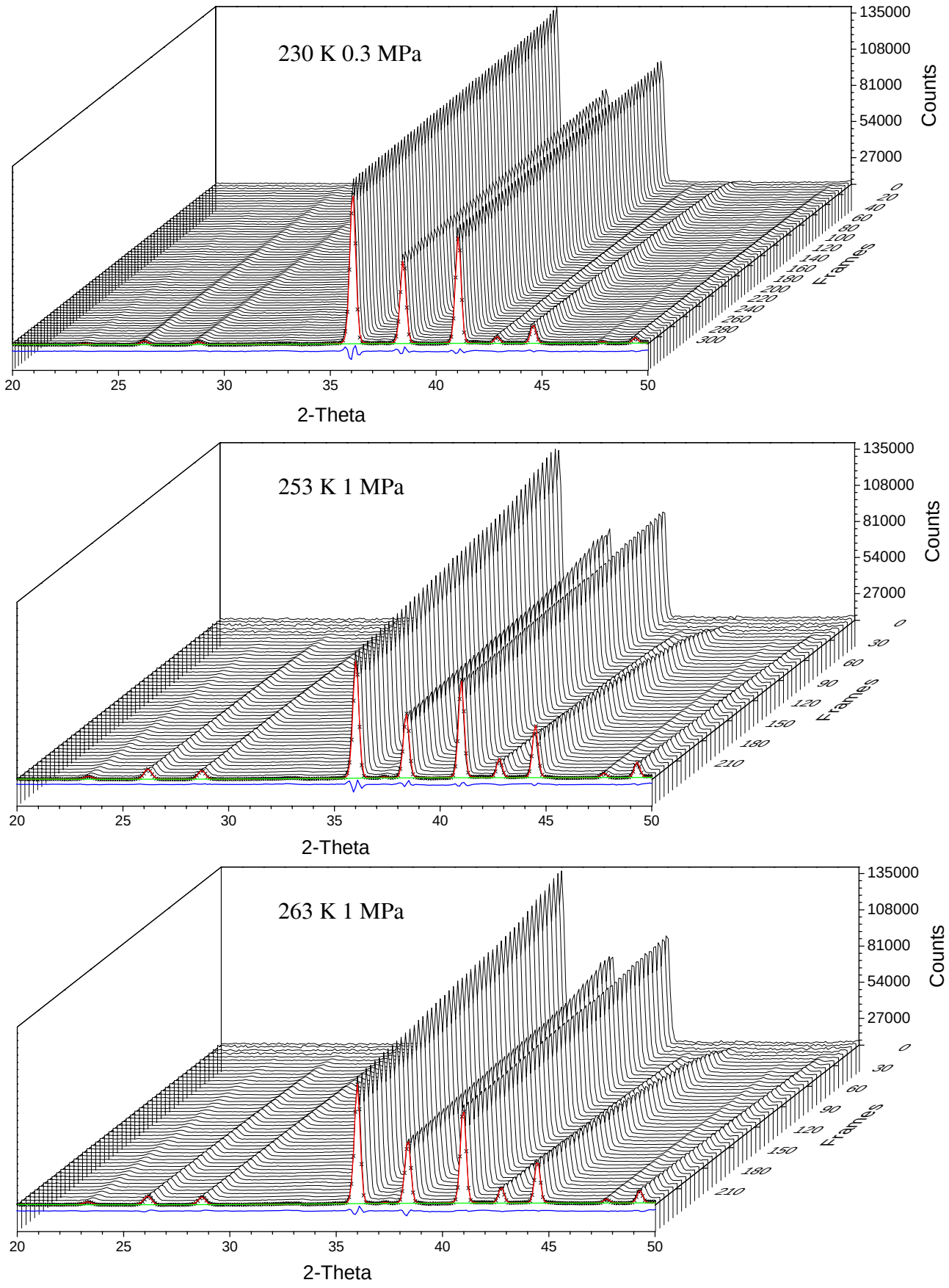

Fig. S1. Series of diffraction patterns (only every 5-th frame is plotted) taken at 230, 253 and 263 K. Last frame is plotted with the Rietveld fit (Red - fitted model, Green- Background, Blue- residual line)

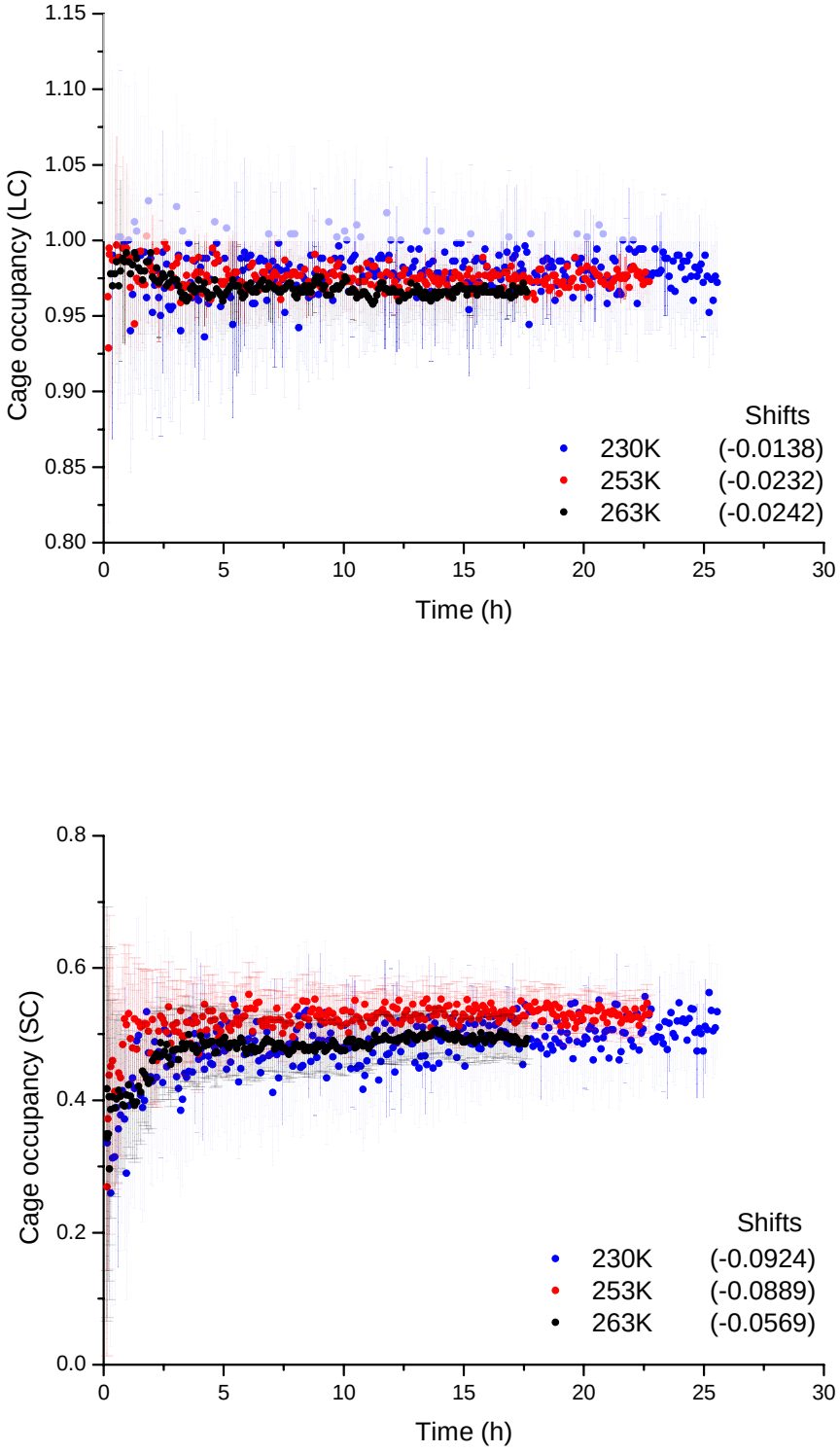

Fig. S2. Time evolution of the gas occupancy for large (LC) and small (SC) cavities in sI CO_2-hydrate. Error bars correspond to 1σ conditional error from the full pattern Rietveld refinement. Shifts of the data sets by the best-fit constant are given in brackets (diffusion-limited scenario). LC occupancy data exceeding 1.0 are unphysical and have been dimmed.

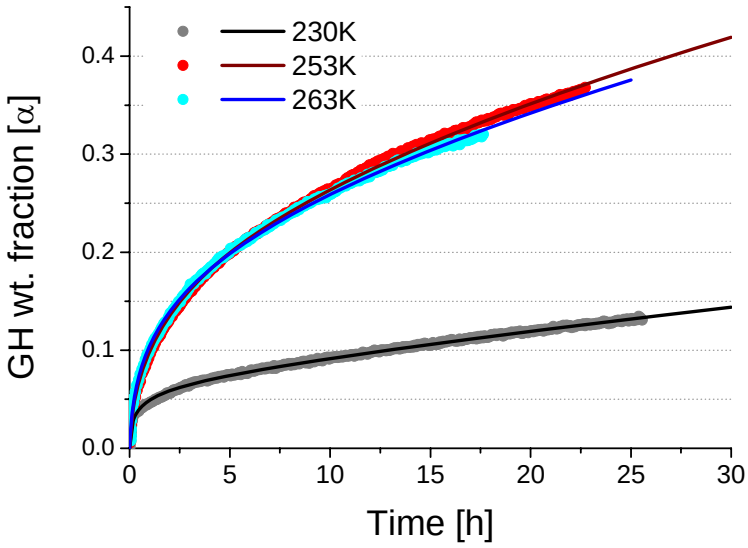

Fig. S3. Kinetics of CO_2-hydrate formation from deuterated ice powder at 263, 253, and 230 K in Runs 1, 2, and 3 (circles) of neutron diffraction experiments and the best-fit kinetic curves (solid lines) simulated by POWDER-5 system in the reaction-controlled scenario.

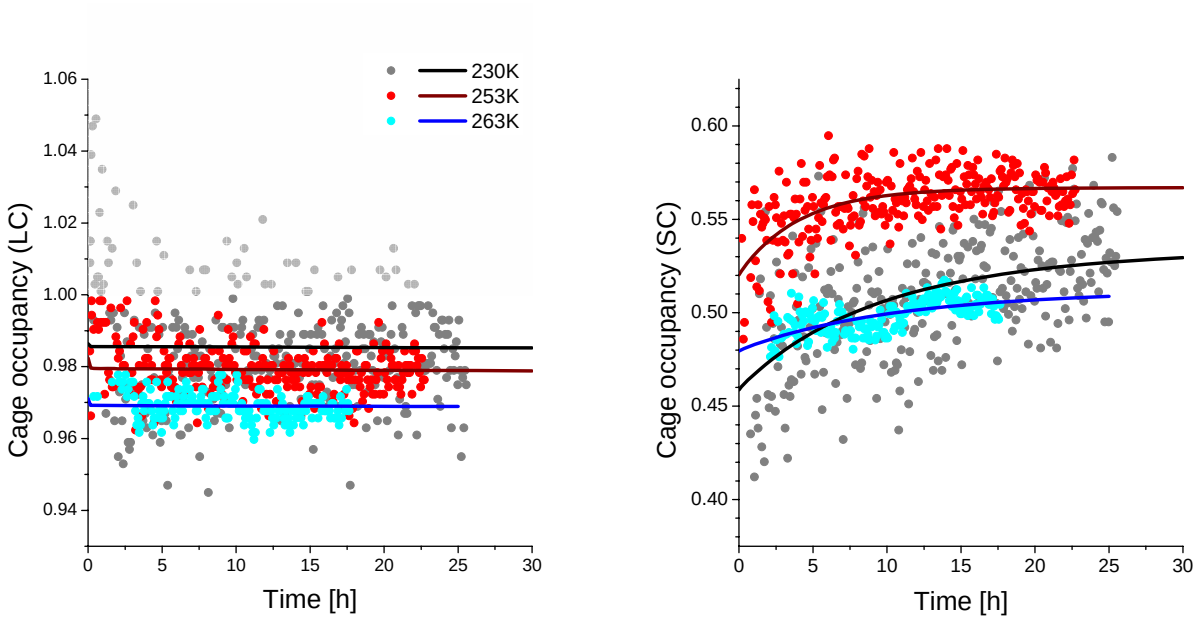

Fig. S4. Occupancy variation versus time for LC-s and SC-s: CO_2-hydrate formation from deuterated ice powder at 263, 253, and 230 K and the best-fit kinetic curves (solid lines) simulated by POWDER-5 system in the reaction-controlled scenario. LC occupancy data exceeding 1.0 are unphysical and have been dimmed.

	230 K	253 K	263K
O (Frame)	0.055717	0.063784	0.066723
D (Frame)	0.056204	0.064271	0.067210
O (LC)	0.172160	0.177927	0.186550
C (LC)	0.139000	0.144767	0.153390
C (SC)	0.043840	0.046230	0.050513
O (SC)	0.075640	0.078030	0.082313

Table. S1. Atomic displacement parameters (ADP-s) used in the Rietveld refinement series. Values are given in U_{iso} format. The full structural model can be found in the supplementary information of [1].

Conditions of experiments				**Deduced kinetic parameters**									
	T K	$p(f)$ MPa	$p_d(f_d)$ MPa	m	k_G m/h$^{m/2}$	σ	k_N 1/h$^{\sigma}$m^2	ϕ_{1h}	χ_g h^{-1}	K_R h^{-1}	D_g m^2/h	D' m^2/h	δ_b, μm
1	263	1.0 (0.93)	0.75 (0.71)	2	$3.5\cdot10^{-3}$	0.5	$1.4\cdot10^{7}$	0.15	7-10	0.034	4.6-4.4·10^{-10}	7.7-7.2(4.3)·10^{-12}	6.6 (6.7)
2	253	1.0 (0.91)	0.51 (0.49)	2	$11\cdot10^{-3}$	0.6	$0.85\cdot10^{7}$	0.3	35	0.016	3.2-3.0·10^{-10}	3.6-3.3(2.1)·10^{-12}	5.4 (4.3)
3	230	0.3 (0.29)	0.186 (0.183)	1.6	$11.5\cdot10^{-4}$	0.4	$1.5\cdot10^{7}$	0.05-0.1	15-20	0.004	1.1-1.0·10^{-10}	8.7-7.7(2.7)·10^{-13}	1.72 (1.33)

Table. S2. Conditions of Experiments and Kinetic Parameters of CO_2-hydrate Formation from Ice Powders. Simulations by the POWDER-5 system with hydrate formation controlled by reaction.

Appendix A. Ice-powder structure evolution during gas-hydrate growth

On average, the local shape of each hydrate layer formed from a single spherical ice grain of initial radius r_{i0} is represented as a truncated sphere of radius r_h (see Fig. A1). The ice core shrinks, its radius r_i decreases, due to the inward growth of the hydrate layer. But, because of the lesser density of water in

the porous hydrate phase, the excess water molecules must be transported to the outward hydrate surface exposed to the ambient gas, and the hydrate layer simultaneously expands into the open space (voids) between the original ice grains. The existing contact areas between neighbouring hydrate shells (ice-hydrate particles) increase, and additional contacts are formed as r_h grows. Correspondingly, the specific surface area of voids S_m and the porosity of the sample ε_m decrease. During stage I of the initial hydrate film formation on ice particles we have to distinguish between the apparent normalized inner and outer hydrate layer radii $R_i = r_i/r_{i0}$ and $R_h = r_h/r_{i0}$ averaged over the whole ice powder surface and their mean relative analogues $\overline{R}_i$, $\overline{R}_h$ under the hydrate coverage.

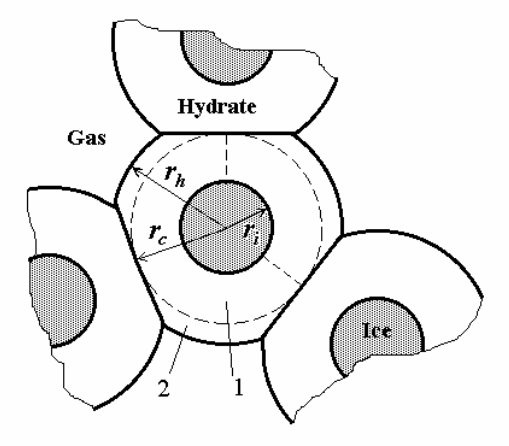

Fig. A1. Schematic of a hydrate layer growing around an ice core in ice powder sample. The spherical boundary of radius r_c, the distance from the ice core centre to an average contact plane, divides the hydrate shell in two sub-layers 1 and 2

In a random dense packing without particle rearrangement, in mono-disperse approximation[2], the current average number of contacts per particle (coordination number) Z can be expressed as a linear function of the relative hydrate shell radius R_h:

$$Z = Z_0 + C(R_h - 1) ,$$

where $Z_0 \sim 7$ is the coordination number of the ice powder and $C \sim 15.5$ is the slope of the random density function.

The normalised volume of a reference ice-hydrate particle is directly related[2, 3] to the reaction degree α or, more precisely, the hydrate layer radius R_h is linked to the radius R_i of the ice – hydrate interface:

$$R_h^{\,3} - \frac{Z_0}{4}(R_h - 1)^2(2R_h + 1) - \frac{C}{16}(R_h - 1)^3(3R_h + 1) = 1 + E\left(1 - R_i^{\,3}\right) ,$$

or equally

$$\frac{dR_h}{dt} = -\frac{ER_i^{\,2}}{sR_h^{\,2}}\frac{dR_i}{dt} ,$$

and by definition

$$\alpha = 1 - R_i^{\,3} .$$

The fraction s of the free hydrate surface area (in units of $4\pi r_h^2$) exposed to the ambient gas and $R_c = r_c/r_{i0}$ are [1, 2]

$$s = 1 - \frac{Z_0}{2}\frac{R_h - 1}{R_h} - \frac{C}{4}\frac{(R_h - 1)^2}{R_h} , \qquad R_c = R_h\left[1 - \frac{2(1-s)}{Z}\right] .$$

These formulas fully describe the local sample structure development on average, during the ice-to-hydrate conversion.

Further, the initial porosity of the ice powder ε_{m0} is directly linked to the structural parameters Z_0 and C, since the quantity $(1 - \varepsilon_{m0})^{-1}$ is the maximum normalised volume, to which the reference ice-hydrate particle can grow, being directly related to the maximum R_h-value, at which $s = 0$. Accordingly, the current porosity ε_m and the normalised surface area of the sample pore space are determined for R_h and s,

$$\varepsilon_m = \varepsilon_{m0} - \alpha(1 - \varepsilon_{m0})E , \quad S_m = sR_h^2 S_{i0} ,$$

where $S_{i0} = 3/(r_{i0}\rho_i)$ is the initial specific surface area of the mono-disperse ice powder.

Appendix B. A kinetic model for initial hydrate film formation on spherical ice particles

Here we follow our recent works[1, 4], and introduce the principal notions of (1) the ice-particle surface fraction α_S covered by hydrate film and/or occupied by developing contacts of growing hydrate layers during the initial coating stage I, (2) the thickness δ_0 of the surface ice layer converted to the initial hydrate shell of thickness $d_0 = \delta_0(1 + E)$, and (3) the ice-sphere coating rate Ω_S, which is, by definition, the fraction of the free (exposed to the ambient gas) ice surface which becomes covered by the newly nucleated hydrate patches during a unit of time. However, unlike in[1], we do not assume any more that the local ice-powder structure evolution is not affected by the previous acts of the hydrate patch nucleation and hydrate growth under the coated area of the powder surface. With this in mind, we use the fraction s of the open particle surface not occupied by the contacts between the hydrate layers and exposed to the ambient gas (see Appendix A) to write at any moment of time t with time-dependent Ω_S,

$$d\alpha_S = (1 - \alpha_S)(\Omega_S - ds/dt)dt$$

and

$$\alpha_S = 1 - \exp\left(-\int_0^t \Omega_S(\tau)d\tau + s - 1\right) \approx 1 - s\exp\left(-\int_0^t \Omega_S(\tau)d\tau\right) . \qquad \text{(B1)}$$

The generalized relation (B1) for α_S reduces to its simplified analogue from[1] at $s = 1$.

Vandermeer-Rath microstructural path methodology[5] assumes that the apparent radius of a hydrate patch develops with its age τ as $2G\tau^{m/2}$, where G is the growth rate constant and the 2-D growth exponent is $m \sim 2$. Correspondingly, the nucleation rate per unit of area varies with time as $N_0 t^{\sigma-1}$, where N_0 is the nucleation rate constant and the exponent σ ranges from 0 to 1 for instantaneous and uniform nucleation, respectively. The refined JMAK approach gives[1] the following parameterization:

$$\int_0^t \Omega_S(\tau)d\tau = \begin{cases} \omega_S \int_0^t \left(\frac{\tau}{t_0}\right)^m (t-\tau)^{\sigma-1} d\tau, \ t < t_0; \\ \omega_S \int_0^{t_0} \left(\frac{\tau}{t_0}\right)^m (t-\tau)^{\sigma-1} d\tau + \frac{\omega_S}{\sigma}(t-t_0)^{\sigma}, \ t > t_0, \end{cases} \qquad \text{(B2)}$$

Here $t_0 = (r_{i0}/G)^{2/m}$ is the typical time needed for a newly nucleated hydrate spot to grow to a maximum-size patch (limited by the ice-sphere surface area), and $\omega_S = 4\pi r_{i0}^2 N_0$ is the nucleation-limited rate of coating. Differentiation of Eq. (B2) with respect to t yields the relationship for Ω_S.

Appendix C. A mass-balance equation of ice-to-hydrate conversion on macro-scale level

If $\Delta_i(t, \tau)$ is the relative mean radius of the ice core (normalized by r_{i0}) at time t under the particle surface area covered by hydrate at a moment τ then[1] the increment of the reaction degree α related to the time interval $d\tau$ is

$$d\alpha = [1 - \Delta_i^{\,3}(t,\tau)]d\alpha_S(\tau) \ ,$$

and

$$\alpha = \int_0^t \left[1 - \Delta_i^{\,3}(t,\tau)\right] d\alpha_S(\tau) \ . \tag{C1}$$

Differentiation of Eq. (C1) with respect to time t yields

$$\frac{d\alpha}{dt} = [1 - \Delta_i^{\,3}(t,t)]\frac{d\alpha_S}{dt} - 3\int_0^t \Delta_i^{\,2}(t,\tau)\frac{d\Delta_i}{dt}(t,\tau)d\alpha_S(\tau) \ . \tag{C2}$$

Next, let us note that during a time period from τ to $\tau + d\tau$ hydrate film was formed only on the free ice surface $d\alpha_F$, and in accordance with Appendix B (see Eq. (B1) at $s = 1$) we have

$$d\alpha_F(\tau) = (1 - \alpha_S)\Omega_S(\tau)d\tau \ .$$

Hence, by definition,

$$[1 - \Delta_i^{\,3}(t,t)]\frac{d\alpha_S}{dt} \approx \frac{3\delta_0}{r_{i0}}\frac{d\alpha_F}{dt} = \frac{3\delta_0}{r_{i0}}(1 - \alpha_S)\Omega_S(t) \ . \tag{C3}$$

Furthermore, we assume the ergodicity of ice-powder structure development in microscopically randomly uniform process of hydrate patch nucleation and growth around ice cores. Thus, the time averaging integral in Eq. (C2) can be expressed in terms of the relative spatially averaged ice-core radius (normalized by r_{i0}) under the inter-particle contacts and hydrate covered area,

$$\overline{R}_i \approx (1 - \alpha/\alpha_S)^{1/3} \ ,$$

to write

$$\int_0^t \Delta_i^{\,2}(t,\tau)\frac{d\Delta_i}{dt}(t,\tau)d\alpha_S(\tau) \approx -\frac{\alpha_S \overline{R}_i^{\,2}\omega_V}{\rho_i r_{i0}} \ . \tag{C4}$$

Here, in Eq. (C4), ω_V designates the mean ice-to-hydrate conversion rate, i.e. the number of ice moles transformed to hydrate on a unit area of ice-hydrate interface per a unit of time.

Finally, substitution of Eqs. (C3) and (C4) into Eq. (C2) results in the mass-balance equation which governs the ice-to-hydrate conversion in ice powders on macro-scale level,

$$\frac{d\alpha}{dt} = S_{i0}[(1-\alpha_S)\rho_i\delta_0\Omega_S + \alpha_S \overline{R}_i^{\,2}\omega_V] \ ,$$

where $S_{i0} = 3/(r_{i0}\rho_i)$ is the initial specific surface area of ice spheres in the sample defined in Appendix A.

It should be emphasized that during stage I of ice surface coating, for $\alpha_S < 1$, $\overline{R}_i$ differs from R_i which is directly linked to the reaction degree $\alpha = 1 - R_i^3$. In our recent study[1] we implicitly assumed $\overline{R}_i \equiv R_i$, setting $s = 1$ in Eq. (B1) in Appendix B, and, thus, neglected the interaction between the ice-surface coating and subsequent hydrate layer growth due to formation and development of inter-particle contacts. This is equivalent to the assumption that the ice-to-hydrate conversion occurs independently in different macroscopic locations of ice powder and might be a good approximation for the low temperature limit controlled by the hydrate film growth.

Appendix D. Finite-difference approximation and computational algorithm for modelling the sI-hydrate layer growth on ice particles

First, we introduce the constant time step h_t and number by index n the states and spatial distributions of different characteristics of the hydrate layer at the time moment $t_n = nh_t$, $n = 0, 1,\ldots$ At any time $t = t_n$, the hydrate layer interval $[\overline{R}_i^{\,n}, \overline{R}_h^{\,n}]$ is discretized by nodes $R = R_j$ numbered by sub-index j counted from $-n$ to n. By definition, $R_0 = 1$, and $R_{-n} = \overline{R}_i^{\,n}$, $R_n = \overline{R}_h^{\,n}$, $n = 1, 2\ldots$ The respective variable spatial steps are $h_j = R_j - R_{j\text{-}1}$, $j = -n+1$ to n. By definition, the initial steps are on the order $h_0 \sim \delta_0/r_{i0}$ and $h_1 \sim E\delta_0/r_{i0}$. They can be additionally sub-divided into smaller intervals (steps) for higher accuracy of computations.

To move to the next time level from t_n to t_{n+1} we write the implicit absolutely stable finite-difference approximation for the gas diffusion equations (14) formulated in our paper:

$$\frac{y_{1\,j}^{\,n+1} - y_{1\,j}^{\,n}}{h_t} = \frac{\nu_2\chi_g}{2(C_1+C_2)}\left[(C_2-C_1)(y_{1\,j}^{\,n+1}y_{2\,j}^{\,n} + y_{1\,j}^{\,n}y_{2\,j}^{\,n+1}) - C_2(y_{1\,j}^{\,n+1} + y_{1\,j}^{\,n}) + C_1(y_{2\,j}^{\,n+1} + y_{2\,j}^{\,n})\right],$$

$$\frac{y_{2\,j}^{\,n+1} - y_{2\,j}^{\,n}}{h_t} + \frac{\nu_1}{\nu_2}\frac{y_{1\,j}^{\,n+1} - y_{1\,j}^{\,n}}{h_t} = \frac{2D_g}{r_{i0}^{\,2}A_j(h_{j+1}+h_j)}\left(A_{j+1/2}\frac{y_{2\,j+1}^{\,n+1} - y_{2\,j}^{\,n+1}}{h_{j+1}} - A_{j-1/2}\frac{y_{2\,j}^{\,n+1} - y_{2\,j-1}^{\,n+1}}{h_j}\right), \tag{D1}$$

$$j = -n,\ldots n.$$

To solve the system of simultaneous linear algebraic equations (D1) one has to deduce the boundary conditions from Eqs. (12), (13), (15), and (16) of the paper in order to determine the occupancies $y_{1\,-(n+1)}^{\,n+1}$, $y_{2\,-(n+1)}^{\,n+1}$ at the clathration front and the steps h_{-n} and h_{n+1}, that is the respective radii $\overline{R}_i^{\,n+1} = R_{-(n+1)}$ and $\overline{R}_h^{\,n+1} = R_{n+1}$. With this in mind, we combine Eqs. (12) and (15) and rewrite them at $t = t_{n+1}$ in the finite-difference representation as

$$K_R\left[\frac{\nu_1}{\nu_1+\nu_2}\ln\frac{1-y_{1-(n+1)}^{\,n+1}}{1-y_{1d}} + \frac{\nu_2}{\nu_1+\nu_2}\ln\frac{1-y_{2-(n+1)}^{\,n+1}}{1-y_{2d}}\right] = -\frac{\nu_2 D_g}{r_{i0}^{\,2}c_{gi}^{\,n+1}}\frac{y_{2-n}^{\,n+1} - y_{2-(n+1)}^{\,n+1}}{h_{-n}} \ , \tag{D2}$$

$$h_{-n} = R_{-n} - R_{-(n+1)} = \overline{R}_i^{\,n} - \overline{R}_i^{\,n+1} = (1-\alpha^n/\alpha_S^{\,n})^{1/3} - (1-\alpha^{n+1}/\alpha_S^{\,n+1})^{1/3} \ .$$

At the same time, Eq. (16) yields

$$h_{n+1} = \frac{E}{2}\left[\frac{1}{s^n}\left(\frac{\overline{R}_i{}^n}{\overline{R}_h{}^n}\right)^2 + \frac{1}{s^{n+1}}\left(\frac{\overline{R}_i{}^{n+1}}{\overline{R}_h{}^{n+1}}\right)^2\right] h_{-n} \ , \tag{D3}$$

while Eq. (12) at $t = t_{n+1}$ directly gives

$$\omega_V{}^{n+1} = -\rho_i r_{i0} K_R \left[\frac{\nu_1}{\nu_1+\nu_2}\ln\frac{1-y_{1-(n+1)}^{n+1}}{1-y_{1d}} + \frac{\nu_2}{\nu_1+\nu_2}\ln\frac{1-y_{2-(n+1)}^{n+1}}{1-y_{2d}}\right] =$$

$$= \frac{\rho_i \nu_2 D_g}{c_{gi}{}^{n+1} r_{i0}} \frac{y_{2-n}^{n+1} - y_{2-(n+1)}^{n+1}}{h_{-n}} \ . \tag{D4}$$

For a given equilibration degree ϕ_{1i}, Eqs. (5) and (13) deliver

$$f_{1i} = f_d + \phi_{1i}(f_{2i} - f_d) \ ,$$

$$y_{1i} = \frac{C_1\left[(1-\phi_{1i})y_{2d}(1-y_{2i}) + \phi_{1i}y_{2i}(1-y_{2d})\right]}{C_2(1-y_{2i})(1-y_{2d}) + C_1\left[(1-\phi_{1i})y_{2d}(1-y_{2i}) + \phi_{1i}y_{2i}(1-y_{2d})\right]} \ ,$$

and we arrive at the system of nonlinear equations (D2)-(D4) with respect to h_{-n}, h_{n+1}, and $\omega_V{}^{n+1}$, $y_{2-(n+1)}^{n+1}$. If $\overline{R}_i{}^n = 0$ at a certain time-step number $n = n_0$ and all ice particles are converted to hydrate at $t = t_n$, instead of Eqs. (D2)-(D4), it is assumed that $\omega_V{}^n = 0$, h_{-n}, $h_{n+1} = 0$, and $y_{2-n_0}^{n+1} = y_{2-(n_0+1)}^{n+1}$ for $n > n_0$.

Correspondingly, in accordance with Eqs. (5), for equilibration degrees ϕ_{1h} and ϕ_{2h} the guest gas fugacities f_{1h} and f_{2h} introduced in the main text describe the initial gas composition (y_{1h} and y_{2h}) of the newly-formed hydrate particle, while the applied gas fugacity f_a imposes the boundary conditions $y_{1\,n+1}^{n+1} = y_{1a}$ and $y_{2\,n+1}^{n+1} = y_{2a}$ at the outer surface of the hydrate layer, at $R = \overline{R}_h{}^{n+1} = R_{n+1}$.

Using the first of Eqs. (D1), one can express $y_{1\,j}^{n+1}$ via $y_{2\,j}^{n+1}$,

$$y_{1\,j}^{n+1} = e_j^n y_{2\,j}^{n+1} + g_j^n \ , \tag{D5}$$

$$e_j^n = \frac{\nu_2 h_t \chi_g}{2(C_1+C_2)}\left[C_1 + (C_2 - C_1)y_{1\,j}^{\,n}\right] \Big/ \left\{1 + \frac{\nu_2 h_t \chi_g}{2(C_1+C_2)}\left[C_2 - (C_2 - C_1)y_{2\,j}^{\,n}\right]\right\} \ ,$$

$$g_j^n = \left[y_{1\,j}^{\,n} + \frac{\nu_2 h_t \chi_g}{2(C_1+C_2)}(C_1 y_{2\,j}^{\,n} - C_2 y_{1\,j}^{\,n})\right] \Big/ \left\{1 + \frac{\nu_2 h_t \chi_g}{2(C_1+C_2)}\left[C_2 - (C_2 - C_1)y_{2\,j}^{\,n}\right]\right\} \ ,$$

$$j = -n, \ldots n.$$

Accordingly, the second of Eqs. (D1) directly results in the system of linear algebraic equations with respect to $y_{2\,j}^{n+1}$

$$a_j^n y_{2\,j-1}^{n+1} - c_j^n y_{2\,j}^{n+1} + b_j^n y_{2\,j+1}^{n+1} = -f_j^n \ , \tag{D6}$$

$$a_j^n = \frac{2D_g h_t A_{j-1/2}}{{r_{i0}}^2 A_j h_j (h_{j+1} + h_j)} \ , \quad b_j^n = \frac{2D_g h_t A_{j+1/2}}{{r_{i0}}^2 A_j h_{j+1} (h_{j+1} + h_j)} \ ,$$

$$c_j^n = 1 + \frac{\nu_1}{\nu_2} e_j^n + a_j^n + b_j^n \ , \quad f_j^n = {y_2}_j^n + \frac{\nu_1}{\nu_2} ({y_1}_j^n - g_j^n) \ , \quad j = -n, \ldots n,$$

that can be resolved by the sweep method. The boundary value $y_{2\,-(n+1)}^{n+1}$ is derived from Eq. (D2) by the standard halving method.

Based on the Euler's method, the conventional implicit finite-difference representation of ordinary differential equation (17) is processed iteratively two times, simultaneously with Eqs. (D2)-(D6), starting from $y_{1\,-(n+1)}^{n+1} = y_{1-n}^n$, $y_{2\,-(n+1`)}^{n+1} = y_{2-n}^n$ and $\overline{R}_i{}^{n+1} = \overline{R}_i{}^n$, $\overline{R}_h{}^{n+1} = \overline{R}_h{}^n$, $s^{n+1} = s^n$, to rise to the next time level t_{n+1}.

The described computational procedure presents a complete "hole-in-cage-wall" diffusion model adapted for numerical implementation in POWDER-5 computer system.

References for Appendices:

1. Falenty, A.; Salamatin, A. N.; Kuhs, W. F., Kinetics of CO_2-Hydrate Formation from Ice Powders: Data Summary and Modeling Extended to Low Temperatures. *Journal of Physical Chemistry C* **2013,** *117* (16), 8443-8457.
2. Arzt, E., The influence of an increasing particle coordination on the densification of spherical powders. *Acta Metallurgica* **1982,** *30* (10), 1883-1890.
3. Staykova, D. K.; Kuhs, W. F.; Salamatin, A. N.; Hansen, T., Formation of porous gas hydrates from ice powders: Diffraction experiments and multistage model. *Journal of Physical Chemistry B* **2003,** *107* (37), 10299-10311.
4. Salamatin, A. N.; Kuhs, W. F. *Formation of porous gas hydrates*, In: Proceedings of the Fourth International Conference on Gas Hydrate (ed. Mori, Y.H.), Yokohama, 2002; pp 766-770.
5. Humphreys, F. J.; Hatherley, M., *Recrystallization and Related Annealing Phenomena*. 1st ed.; Pergamon Press: Oxford, UK, 2002.